applied sciences

MDPI

Article

16.3 W Peak-Power Pulsed All-Diode Laser Based Multi-Wavelength Master-Oscillator Power-Amplifier System at 964 nm

Thi Nghiem Vu [1,2,3,*], Tran Quoc Tien [2,3], Bernd Sumpf [1], Andreas Klehr [1], Jörg Fricke [1], Hans Wenzel [1,*] and Günther Tränkle [1]

[1] Ferdinand-Braun-Institut gGmbH, Leibniz-Institut für Höchstfrequenztechnik, Gustav-Kirchhoff-Str. 4, 12489 Berlin, Germany; bernd.sumpf@fbh-berlin.de (B.S.); klehr-andreas@t-online.de (A.K.); Joerg.Fricke@fbh-berlin.de (J.F.); guenther.traenkle@fbh-berlin.de (G.T.)

[2] Institute of Materials Science, Vietnam Academy of Science and Technology, 18 Hoang Quoc Viet Rd., Cau Giay, Hanoi 100000, Vietnam; tientq@ims.vast.ac.vn

[3] Graduate University of Science and Technology (GUST), Vietnam Academy of Science and Technology, 18 Hoang Quoc Viet Rd., Cau Giay, Hanoi 100000, Vietnam

* Correspondence: nghiemvt@ims.vast.ac.vn (T.N.V.); hans.wenzel@fbh-berlin.de (H.W.); Tel.: +84-2438360887 (T.N.V.)

Abstract: An all-diode laser-based master oscillator power amplifier (MOPA) configuration for the generation of ns-pulses with high peak power, stable wavelength and small spectral line width is presented. The MOPA emits alternating at two wavelengths in the spectral range between 964 nm and 968 nm, suitable for the detection of water vapor by absorption spectroscopy. The monolithic master oscillator (MO) consists of two slightly detuned distributed feedback laser branches, whose emission is combined in a Y-coupler. The two emission wavelengths can be adjusted by varying the current or temperature to an absorption line and to a non-absorbing region. The power amplifier (PA) consists of a ridge-waveguide (RW) section and a tapered section, monolithically integrated within one chip. The RW section of the PA acts as an optical gate and converts the continuous wave input beam emitted by the MO into a sequence of short optical pulses, which are subsequently amplified by the tapered section to boost the output power. For a pulse width of 8 ns, a peak power of 16.3 W and a side mode suppression ratio of more than 37 dB are achieved at a repetition rate of 25 kHz. The measured spectral width of 10 pm, i.e., 0.1 cm^{-1}, is limited by the resolution of the optical spectrum analyzer. The generated pulses emitting alternating at two wavelengths can be utilized in a differential absorption light detection and ranging system.

Keywords: Y-branch DFB laser; MOPA; ns pulse; DIAL; water vapor

Citation: Vu, T.N.; Tien, T.Q.; Sumpf, B.; Klehr, A.; Fricke, J.; Wenzel, H.; Tränkle, G. 16.3 W Peak-Power Pulsed All-Diode Laser Based Multi-Wavelength Master-Oscillator Power-Amplifier System at 964 nm. *Appl. Sci.* **2021**, *11*, 8608. https://doi.org/10.3390/app11188608

Academic Editor: Hao-chung Kuo

Received: 9 August 2021
Accepted: 13 September 2021
Published: 16 September 2021

1. Introduction

The knowledge of the distribution of atmospheric water vapor and its rapid variations is key information for both weather forecast and climate science [1]. A promising technique for measuring the water vapor distribution with good accuracy and high spatial resolution is differential absorption LIDAR (DIAL), where alternating laser pulses at different wavelengths are utilized. One emission wavelength is set within an absorption line (online wavelength—λ_{on}), and the other one nearby to a non-absorbing spectral range (offline wavelength—λ_{off}). From the time delay between the outgoing pulses and the backscattered signals, the distance to scatterers can be determined. Besides real-time detection, post-processing of the returned signals allows also to characterize the spatial distribution of the water [2]. The DIAL technique has the advantage that the knowledge of the absorption cross sections suffices for the determination of the water vapor density from the ratio of the returned intensities at the online and offline wavelengths. However, the DIAL technique requires a pulsed laser with high wavelength stability and small spectral

linewidth, capable of operating at two different wavelengths. The spectral linewidth of the laser must be at least smaller than the width of the absorption line at atmospheric pressure. Assuming a pressure broadening at normal pressure of 0.1 cm^{-1} measured as full-width at half-maximum (FWHM), this leads to a maximal width of about 10 pm. To maintain low systematic errors, the emission linewidth should be about one order of magnitude smaller, e.g., 1.2 pm (< 400 MHz), reported by Ismail and Browell [3]. Potential absorption bands for the detections are in the spectral regions around 720, 820, 930 and 973 nm [4–6]. The peak power of the pulses should exceed 10 W, providing sufficient backscattered intensity in the case of a ground-based measurement.

The development of DIAL has been strongly connected with the progress in laser technology. Initial modeling indicated that a low pulse energy with a high pulse repetition rate is suitable to measure the water vapor profile in the lower troposphere [7]. This opened the possibility to use all-diode laser-based transmitters in DIAL instruments for inexpensive and reliable water vapor profiling.

Advanced internally wavelength-stabilized diode lasers, such as distributed feedback (DFB) lasers or distributed Bragg reflector (DBR) lasers, provide a stabilized wavelength, a high spectral purity, and are stable against mechanical and thermal disturbances. Both DFB and DBR lasers can operate mode-hop free with a small spectral line width and excellent side mode suppression ratio (SMSR). Their emission wavelengths can be tuned by changing the injection current or temperature. They fulfill not only the requirements for ground-based water vapor DIAL, but also those for space-borne online/offline injection seeders for laser transmitters. Semiconductor optical amplifiers can be used to generate and subsequently amplify optical pulses.

In 2004, the first diode-laser-based water vapor DIAL was demonstrated by Machol et al. [8], using a DFB laser and a flared amplifier operating around 823 nm. By changing the current injected into the DFB laser, online and offline wavelengths were generated. A peak power of 0.5 W with a pulse width of 600 ns at a repetition frequency of 8 kHz was obtained. For faster switching between the two wavelengths, several groups developed DIAL systems, utilizing two diode lasers for the online and offline wavelengths, either DFB lasers [9] emitting near 820 nm or distributed Bragg reflector (DBR) lasers [10–15] emitting near 830 nm. The usage of semiconductor optical amplifiers was demonstrated, too. For example, Repasky et al. [10] developed a laser transmitter, utilizing two DBR lasers and a pulsed tapered semiconductor optical amplifier (TSOA) to generate a peak power of 10 W with a pulse width of 1000 ns at a repetition frequency of 10 kHz around 828 nm. Spuler et al. [11–14] developed a DIAL system based on two single DBR lasers and a TSOA emitting at 830 nm, having a peak power of 5.6 W within 900 ns at 9 kHz.

Common to these references [8–15] is the use of diode laser transmitters having an optical peak power of about 5 to 10 W with a pulse width of 900 ns to 1000 ns at a repetition rate of 6 to 10 kHz. To overcome the necessity of using two diode lasers as seed sources, in this work, we tested the implementation of a dual wavelength Y-branch DFB-laser as the master oscillator (MO) in a master-oscillator power-amplifier (MOPA) configuration recently reported [16,17] based on a continuous-wave (CW) operated MO and a pulsed-driven power amplifier (SA) with an integrated optical gate. At wavelengths of 1060 nm and 975 nm, optical peak powers of 16 W were obtained for pulse widths of τ = 2 ns and τ = 8 ns, respectively, at repetition rates of f = 25 kHz. In this paper, a Y-branch DFB RW laser [18] is used as the master oscillator. In contrast to Y-branch DBR RW lasers [19,20], DFB lasers offer the chance for a fast fine-tuning of the emission wavelength directly by varying the current, whereas DBR lasers can be only tuned by changing the grating temperature.

To demonstrate the potential suitability of the device for the measurement of water vapor using the DIAL technique, the laser was selected to emit in the 964 nm to 968 nm range. Although the wavelengths are in the range of water vapor rotational-vibrational bands [21], the experiments were more focused on the spectral properties and the electro-optical characterization of the MOPA device than on the concrete realization of a ready-to-use device for DIAL.

The MOPA system presented in this work is based on a Y-branch DFB laser operated in CW mode and a pulse-driven two-section PA. Alternating dual wavelength operation was obtained between 964 nm and 968 nm with a measured spectral linewidth below 10 pm and a peak power of more than 10 W. Limited by the available electronics, which was directly connected to the power amplifier, a repetition rate of 25 kHz was used, and a pulse width of 8 ns was obtained.

In what follows, the devices and the MOPA configuration are shortly described. Then, the experimental power-voltage-current characteristics and the spectral properties of the two branches of the Y-DFB laser as well as the temporal and spectral behavior of the output power of the MOPA system are discussed.

2. Devices and Experimental Setup

A scheme of a Y-branch DFB laser is shown in Figure 1. The vertical layer structure grown on an n-GaAs substrate in one epitaxial step is given in Figure 1a. It includes an n- GaAs substrate, n-$Al_{0.35}Ga_{0.65}As$ cladding, 1.6 µm n-$Al_{0.25}Ga_{0.75}As$ waveguide, double quantum well (QW) active region consisting of InGaAs QWs and GaAsP barriers, 0.8 µm p-$Al_{0.25}Ga_{0.75}As$ waveguide, p-$Al_{0.85}Ga_{0.15}As$ cladding and finally, p-GaAs contact layer.

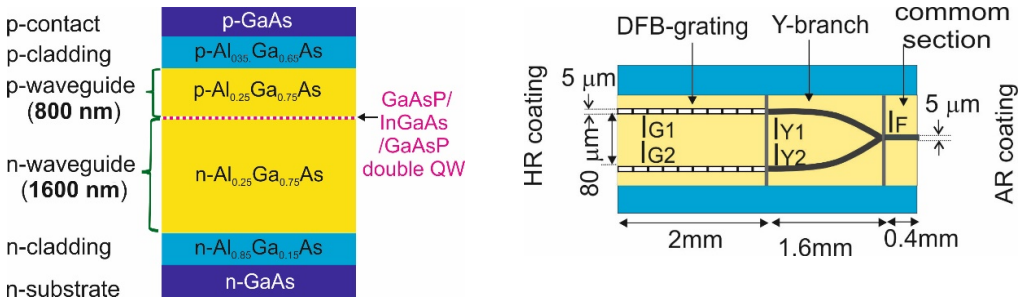

Figure 1. Epitaxial layer structure (**a**) and top view (**b**) of the Y-branch DFB laser.

The lateral–longitudinal structuring starts with the definition of 80th order Bragg gratings in the DFB lasers by i-line wafer stepper lithography. Subsequently, the gratings are transferred by reactive ion etching through the p-cladding into the p-waveguide layer. The use of surface gratings avoids the need for sophisticated grating overgrowth. The large periods of the Bragg grating of about 11.5 µm are used to enable the realization of the current injection between the etched grating grooves. The effective duty cycle of the grating (ratio between unetched region to period) is extremely large (~0.99). In order to achieve good laser performance, a coupling-coefficient length product $\kappa L = 0.3 \ldots 0.5$ is aimed at, where κ is the coupling coefficient of the grating and L is its length, which is achieved by a proper adjustment of the etch depth. The exact grating periods are 11,520.0 nm and 11,567.6 nm to ensure emission wavelengths of around 964 nm and 968 nm, respectively, with an intended spacing of 4 nm.

A top view of the Y-branch DFB laser is shown in Figure 1b. The 4 mm long device consists of two branches and three sections, all of them electrically separated, enabling currents I_{G1}, I_{G2} to each DFB laser, I_{Y1}, I_{Y2} to each S-bend of the Y-coupler and a current I_F to the section at the front facet. The section lengths are 2.0, 1.6 and 0.4 mm for the DFB lasers, Y-coupler and the front section, respectively. Lateral waveguiding is provided by a ridge waveguide with a width of the ridge of 5 µm. The spatial distance between the DFB lasers is 80 µm. Details of the devices manufactured are described in Refs. [18,22,23]. The Y-branch-DFB laser is mounted p-side up on a standard C-mount.

The power amplifier (PA) schematically shown in Figure 2 consists of n-GaAs substrate, n-$Al_{0.45}Ga_{0.55}As$ cladding, 4 µm n-$Al_{0.35}Ga_{0.65}As$ waveguide, InGaAs/GaAsP double quantum well as the active region, 0.8 µm p-$Al_{0.35}Ga_{0.65}As$ waveguide, p-$Al_{0.85}Ga_{0.15}As$ cladding and p-GaAs contact layer (Figure 2a). The asymmetrical super large optical cavity

results in a small vertical far-field divergence of only 14° full-width at half maximum (FWHM) [24,25].

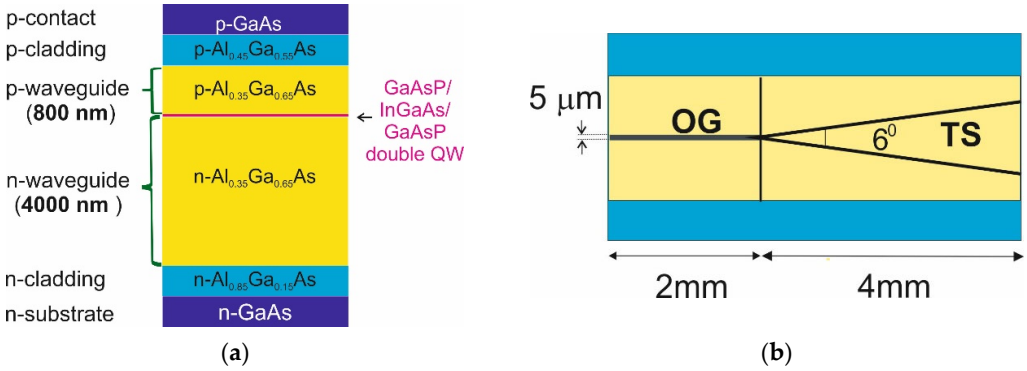

Figure 2. Epitaxial layer structure (**a**) and top view (**b**) of the power amplifier with integrated optical gate (OG) and tapered section (TS).

The PA has a total length of 6 mm and consists of two electrically separated sections, namely, a 2 mm long index-guided RW section having a 4 µm wide ridge and a 4 mm long gain-guided tapered section (TS) having a full flare angle of 6° (Figure 2b). The front and the rear facets are passivated and anti-reflection coated to achieve a residual reflectivity of $R \leq 5 \times 10^{-4}$ in the spectral range from 950 nm to 980 nm. The device is mounted p-side up on a C-mount, allowing to drive the two sections electrically independent from each other. The electro-optical characteristics were investigated in detail in [17]. An average power of 1.4 mW or a pulse power of 3.8 W of amplified spontaneous emission (ASE) was reached if a current pulse with a length of τ_{TS} = 15 ns and an amplitude of I_{TS} = 18.4 A was injected into the TS at a repetition rate of f = 25 kHz and a temperature of T = 30 °C. The peak wavelength and 3 dB full width of the ASE spectrum were about λ = 969 nm and 18 nm, respectively. No lasing modes were observed.

The experimental setup of the MOPA configuration under study is shown in Figure 3. The emission from the Y-branch DFB laser, used as MO, is collimated with an anti-reflection coated aspheric lens having a focal length of 3.1 mm and a numerical aperture (NA) = 0.68 (Thorlabs; 352330-B). The light passes a two-stage optical isolator (60 dB isolation; Qioptiq FI-1060-TI) and is focused, using another aspheric lens (Thorlabs; 352330-B) into the OG section of the power amplifier. To obtain stable online/offline wavelength pairs in the 964 nm range with a small spectral linewidth, the MO is operated in CW mode.

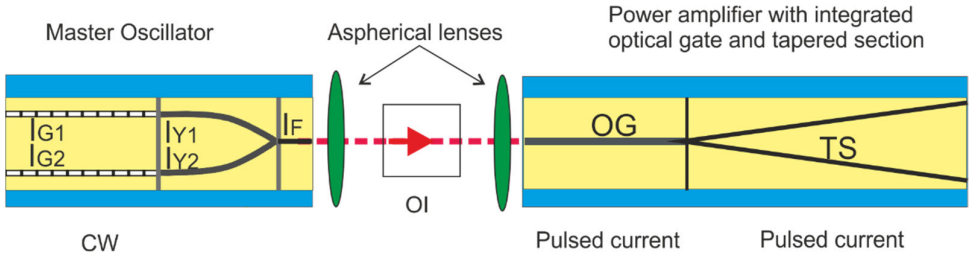

Figure 3. Scheme of experimental MOPA configuration.

The RW section and the TS of the PA are operated in pulsed mode for generating optical pulses with high peak power and low ASE. The RW section of the PA shown in Figure 3 serves as an optical gate (OG), where the coupled CW beam of the MO is absorbed if no current is injected. On the other hand, the OG becomes transparent, and the optical beam can pass the OG if a current pulse of defined width τ_{OG} and amplitude I_{OG} is injected. In this work, the amplitude of the current pulse is I_{OG} = 100 mA. The generated optical pulse is then subsequently amplified in the tapered section, where a current with

an amplitude of $I_{TS} \leq 18.4$ A is injected. Due to the targeted optical pulse width of 8 ns a pulse width of $\tau_{OG} = 8$ ns for the gate current is chosen. To obtain a top-hat profile of the optical pulse, the pulse width τ_{TS} has to be longer than τ_{OG}, but not too long in order to prevent the generation of ASE after the emission of the optical pulse. The time needed to accumulate enough excess carriers in the active region amounts to several times the carrier lifetime, which is of the order of 1 ns. Hence, the electrical pulse injected into the TS is turned on 3.5 ns before the pulse through the OG is injected as discussed in Refs. [16,17]. Thus, the pulse injected into the OG is delayed by a time $\tau_{Delay} = 3.5$ ns with respect to the TS pulse. Similarly, the TS pulse is kept on for a further 3.5 ns after turning off the OG pulse. Therefore, a pulse width of $\tau_{TS} = 15$ ns is selected. The repetition rate of the current pulses injected into both sections (OG and TS) is $f = 25$ kHz. The current pulses injected into the OG and the TS are generated by driver circuits based on GaN transistors as described in Ref. [26]. In the following, the electro-optical characteristics, including the spectral properties of the MO as well as the MOPA configuration are given.

3. Experimental Results

The dependence of the optical power and the voltage versus the currents I_{G1} and I_{G2} injected into the two DFB lasers are shown in Figure 4a for $T = 25$ °C and 35 °C. These temperatures enable the selection of two adequate pairs of online and offline wavelengths. The current to the front section is set to $I_F = 10$ mA, whereas the currents to the Y-coupler are set to $I_{Y1} = I_{Y1} = 0$ mA to avoid crosstalk between both branches. Thus, the Y-coupler is optically pumped to near transparency, which is possible because of low non-saturable optical losses, due to a free carrier absorption if the order 1 cm^{-1} and the absence of intervalence-band absorption as well as high differential gain and low transparency carrier density of the compressively strained InGaAs QWs. At currents of 250 mA and at $T = 25$ °C, output powers of $P = 96$ mW and 93 mW are reached for each branch. At $T = 35$ °C, the optical power decreases to 90.0 mW and 86.6 mW. The slope efficiency is 0.60 W/A at 25 °C and 0.57 W/A at 35 °C for the first branch and 0.54 W/A at 25 °C and 0.50 W/A at 35 °C for the second branch.

Optical spectra are measured with an optical spectrum analyzer (OSA) having a resolution of 10 pm and a dynamic range of 60 dB (Advantest Q8384). Figure 4b shows the optical spectra having peak wavelengths of 940.02 nm and 967.50 nm at a current of $I_{G1} = I_{G2} = 130$ mA corresponding to a power of about 30 mW, later used as input power for the MOPA system. A side-mode suppression ratio (SMSR) of about 55 dB and a spectral full 3 dB width of 10 pm (limited by the OSA) are obtained.

The dependence of the optical spectra on the injection current to the two branches with fixed $I_F = 10$ mA and $I_{Y1} = I_{Y2} = 0$ mA is shown in Figure 4c as a pseudo-color mapping at $T = 25$ °C and $T = 35$ °C. Each DFB laser branch operates in a single longitudinal mode over the whole current range from 80 mA to 250 mA with a constant distance between the two peak wavelengths of 3.48 nm. It is smaller than the designed value (4 nm) probably since the dispersion of the effective index is not considered in the design of the grating periods. The increase of the peak wavelength with rising current is caused by self-heating, which leads to an increase in the modal refractive index and thus, in the Bragg wavelength. At $T = 25$ °C, the tuning range, due to a change in the current from 80 mA to 250 mA, is 0.13 nm, corresponding to 0.52 pm/mA for both branches, i.e., from 964.02 nm to 964.15 nm for the first branch and from 967.42 nm to 967.56 nm for the second one. At $T = 35$ °C, the corresponding tuning ranges are 964.29–964.42 nm and 967.75–967.88 nm, respectively.

As shown in [15], the output power of the PA remains almost constant when the input power varies in the range between 15 mW and 50 mW. In this work, an input power of about 20 mW corresponding to currents $I_{G1} = I_{G2} = 130$ mA is chosen. The PA is operated at $\tau_{OG} = 8$ ns, $I_{OG} = 100$ mA, $\tau_{Delay} = 3.5$ ns, $\tau_{TS} = 15$ ns, $I_{TS} = 18.4$ A, $f = 25$ kHz, $T_{PA} = 25$ °C.

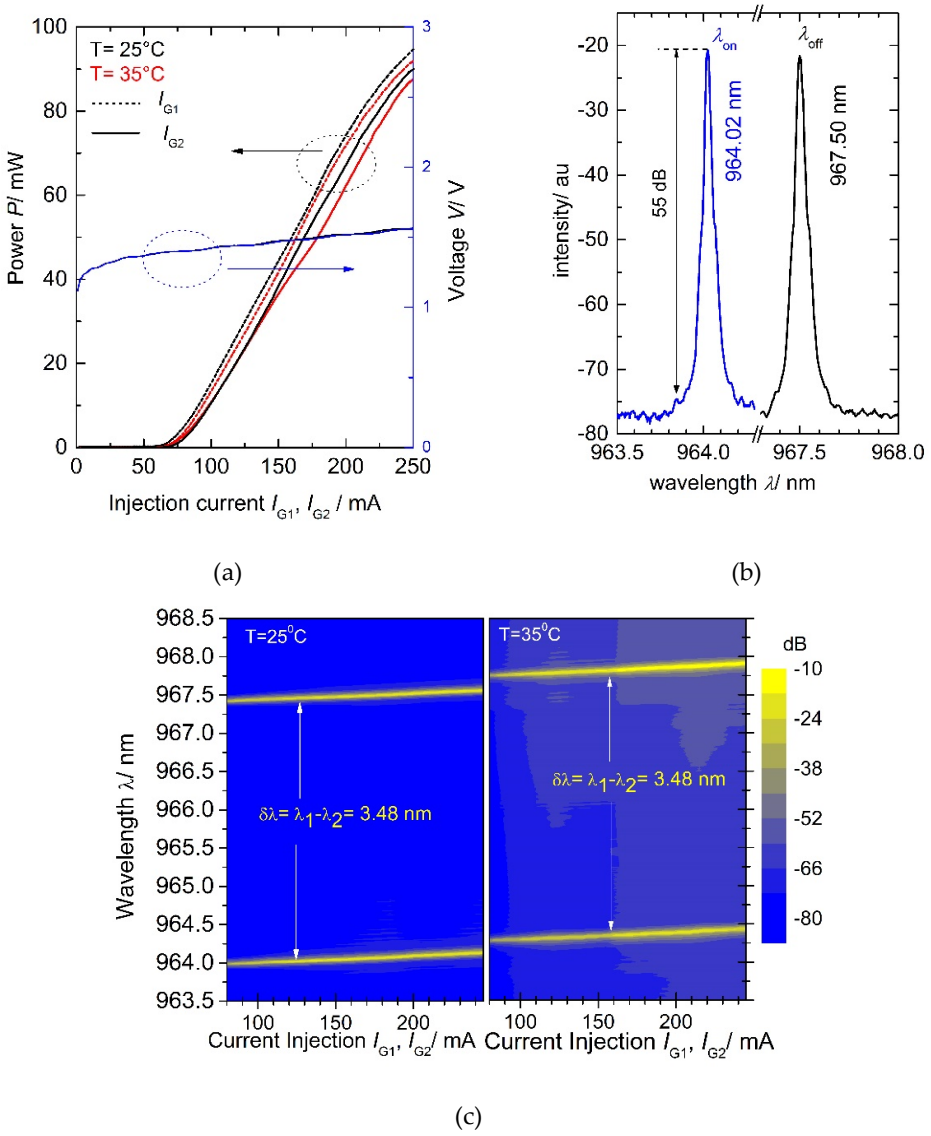

Figure 4. (**a**) CW optical output power (left axis) and voltage (right) versus the injection currents to the two branches of the Y-DFB laser (I_{G1}: dotted lines, I_{G2}: solid lines) at T = 25 °C (black) and 35 °C (red). (**b**) CW optical spectra of the two branches at currents of I_{G1} = I_{G2} = 130 mA at T = 25 °C. (**c**) Superimposed pseudo-color mappings of CW optical spectra of the two branches in dependence on the injection currents at T = 25 °C (left) and T = 35 °C (right).

The results for a seed wavelength of 964.02 nm, corresponding to an operation of the first branch of the Y-DFB laser (I_{G1} = 130 mA, I_{G2} = 0 mA), are shown in Figure 5. An optical pulse width of 8 ns and a plateau optical peak power of the MOPA system of 16.3 W is obtained. At the leading and training edges of the optical pulse, small amounts of ASE are visible in Figure 5a.

The dependence of the time-averaged optical spectra of the MOPA on the current I_{TS} is shown in Figure 5b as a color-scale mapping. Over the whole range of TS currents, the peak wavelength of the MOPA does not change and the spectral width remains < 10 pm because of the fixed seeding wavelength. A comparison between optical spectra emitted by the DFB laser at $P \approx 20$ mW and the MOPA at P = 16.3 W is given in Figure 5c. The peak wavelength of 964.02 nm and the measured spectral full width at half maximum (FWHM) below 10 pm given by the resolution limit of the optical analyzer coincide for both the MO and the MOPA. The side mode suppression ratio (SMSR) of 55 dB of the DFB laser is larger

than that of the MOPA, where the ASE leads to a deterioration of the SMSR to 40 dB, which is still an excellent value for such a MOPA device.

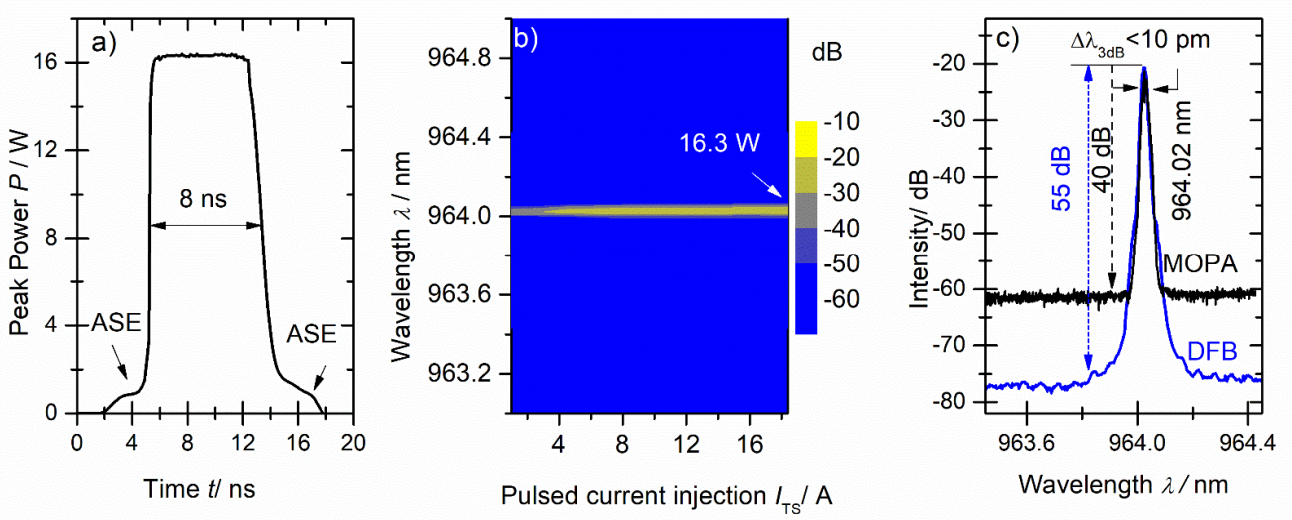

Figure 5. (**a**) Temporal behavior of the optical power emitted by the MOPA system at a seed wavelength of 964.02 nm, (I_{G1} = 130 mA, I_{G2} = 0 mA). (**b**) Color-scale mapping of the time-averaged optical spectrum of the MOPA in dependence of the amplitude of the current pulses injected into the TS for a fixed DFB laser current of I_{G1} = 130 mA, I_{G2} = 0 mA. (**c**) Comparison between the optical spectra of the DFB laser and the MOPA system for I_{G1} = 130 mA, I_{G2} = 0 mA and I_{TS} = 18.4 A.

The results for a seeding wavelength of 967.50 nm, corresponding to an operation of the second branch of the Y-DFB laser (I_{G1} = 130 mA, I_{G2} = 0 mA) shown in Figure 6 are very similar to those shown in Figure 5. When changing the temperature to T_{MO} = 35 °C and fixing all other conditions, the same optical peak power of 16.3 W for the wavelength pair 964.33 nm and 967.81 nm is obtained (not shown here).

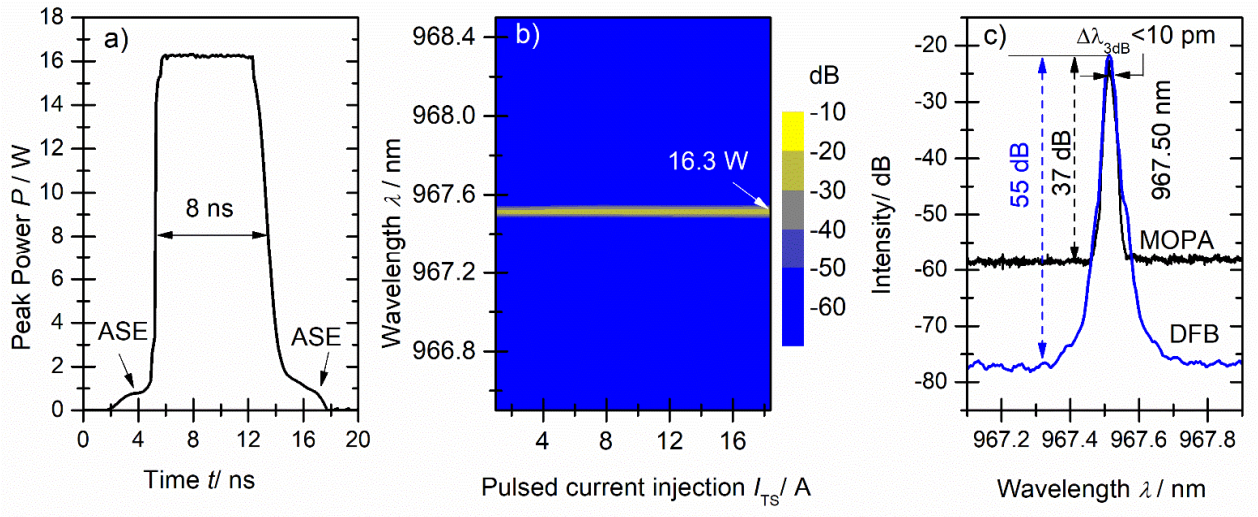

Figure 6. (**a**) Temporal behavior of the optical power emitted by the MOPA system at a seed wavelength of 967.50 nm (I_{G1} = 130 mA, I_{G2} = 0 mA). (**b**) Color-scale mapping of the time-averaged optical spectrum of the MOPA in dependence of the amplitude of the current pulses injected into the TS for a fixed DFB laser current of I_{G1} = 0 mA, I_{G2} = 130 mA. (**c**) Comparison between the optical spectra of the DFB laser and the MOPA system for I_{G1} = 0 mA, I_{G2} = 130 mA and I_{TS} = 18.4 A.

The widths of the optical spectra given in this paper are limited by the resolution of the optical spectrum analyzer (Advantest Q8384) used. It can be expected that the true spectral

linewidths are significantly smaller. Indeed, CW-operated DFB and DBR lasers emitting at 1064 nm having similar epitaxial layer structures, ridge waveguides and cavity lengths measured by the self-delayed heterodyne measurement technique in our lab revealed spectral linewidths below 1 MHz (0.003 pm), using commercially available low-noise current sources. For the DFB laser, a minimum intrinsic (Lorentzian) linewidth of 22 kHz and a total (FWHM) linewidth of 234 kHz were found [27]. A DBR laser exhibited even smaller values of 2 kHz (intrinsic linewidth) and 180 kHz (total linewidth) [28]. Although the spectral linewidth is not deteriorated by the PA as shown in [29] for a CW operated PA, in our case, the optical spectrum is enlarged since the Fourier transform limit of an 8 ns long pulse is of the order 100 MHz (0.3 pm). The SMSR is deteriorated too because of the additional ASE emitted by the PA.

In Figure 7, the dependence of the optical spectra of the MOPA on the pulse current I_{TS} injected into the tapered section (I_{TS} = 4, 8, . . . ,18.4 A) is shown. It can be clearly seen that the intensity of the ASE increases with rising I_{TS} but the spectral shape of the mode remains almost constant.

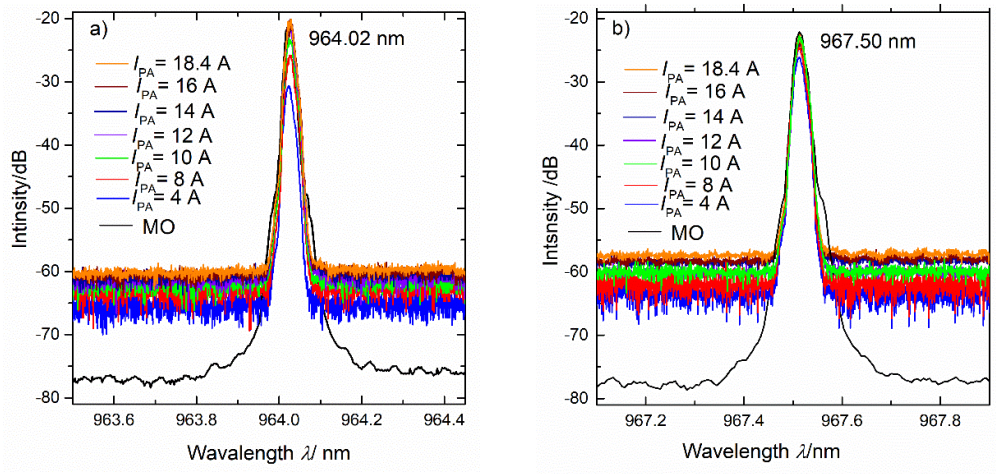

Figure 7. Time-averaged optical spectra of the MO (black curves) and the MOPA (colored curves) for different pulse currents as indicated in the legends emitted by the left (**a**) and right (**b**) branches of the Y-DFB laser.

Although we did not measure the spatial beam properties of the MOPA system, we know from CW operated tapered amplifiers that they emit a near diffraction limited beam if the input beam is diffraction limited. For example, in Ref. [30] a lateral beam quality factor M^2 = 1.7 was measured for a 3 mm long amplifier at a CW output power of 4.5 W.

In this study, we use a repetition frequency of 25 kHz corresponding to a duty cycle of only 0.02% for a pulse width of 8 ns. An increasing repetition frequency results in a larger duty cycle and hence, in a rise in the average thermal load, which could have an impact on both the performance of the driver circuit and the amplifier. However, we believe that repetition frequencies of several 100 kHz are still feasible because the time-averaged thermal load of the PA is of the order of only 100 mW, assuming a conversion efficiency of 30%.

These properties prove that the concept of using a wavelength-stabilized diode laser emitting two wavelengths alternating in CW mode and a pulsed-driven multi-section tapered amplifier is well suited to be utilized for DIAL measurements of water vapor in the atmosphere. A correspondingly tailored laser source would be capable of providing high-peak power, small spectral line widths and rapid wavelength switching by applying the current of a driver circuit capable to provide ns-pulses to our monolithic MO.

4. Summary and Outlook

Nanosecond optical pulses at two alternating wavelengths between 964 nm and 968 nm were generated, using a MOPA system consisting of a Y-branch DFB laser and a power amplifier with an integrated optical gate and tapered section. The Y-branch DFB laser was operated in CW mode, while the optical gate and the tapered section were operated in pulsed mode. The spectral properties of the MOPA are governed by the MO and the Fourier transform limit of the generated pulses. The measured spectral widths below 10 pm, limited by the resolution of the OSA, remained constant at all output power levels of the MOPA system. A true spectral line width of the order of 100 MHz (0.3 ps) for 8 ns long pulses, given by the Fourier transform limit, can be expected. A maximum optical peak power of 16.3 W and a SMSR of 37dB were obtained for a pulse width of 8 ns. These parameters show the potential suitability of the light source concept for the measurement of water vapor, using the DIAL technique. Further studies will include measurements of the spatial beam properties and the spectral linewidth of the MOPA system. The attachment of a fast driver circuit would enable a rapid switching between the wavelengths of the two DFB branches in our monolithic MO. A field test of differential absorption LIDAR measurement will be performed in future to confirm the advantage of the system in water vapor detection.

Author Contributions: Conceptualization, B.S., A.K., T.Q.T. and G.T.; methodology, A.K. and T.N.V.; Investigation, T.N.V. and J.F.; supervision, writing—original draft, writing—review and editing, T.N.V., H.W., B.S., J.F. and G.T. All authors have read and agreed to the published version of the manuscript.

Funding: This research was funded by Institute of Materials Science, Vietnam Academy of Science & Technology under Grant Number CS.16/20-21.

Institutional Review Board Statement: Not applicable.

Informed Consent Statement: Not applicable.

Data Availability Statement: The data can be received from the authors on request.

Acknowledgments: T.N.V.; A.K. and B.S., acknowledge the technical support by J. Hopp and A. Ginolas.

Conflicts of Interest: The authors declare no conflict of interest.

References

1. Schneider, T.; O'Gorman, P.A.; Levine, X.J. Water vapor and the dynamics of climate changes. *Rev. Geophys.* **2010**, *48*, 3. [CrossRef]
2. Collis, R.T.H.; Russell, P.B. Lidar measurement of particles and gases by elastic backscattering and differential absorption. In *Laser Monitoring of the Atmosphere*; Springer: Berlin/Heidelberg, Germany, 1976; pp. 71–151.
3. Ismail, S.; Browell, E.V. Recent lidar technology developments and their influence on measurements of tropospheric water vapor. *J. Atmos. Ocean Technol.* **1994**, *11*, 76–84. [CrossRef]
4. Cahen, C.; Megie, G. A spectral limitation of the range resolved differential absorption lidar technique. *J. Quant. Spectrosc. Radiat. Transfer* **1980**, *25*, 151–157. [CrossRef]
5. Chu, Z.; Wilkerson, T.D.; Singh, U.N. Water-vapor absorption line measurements in the 940-nm band by using a Raman-shifted dye laser. *Appl. Opt.* **1993**, *32*, 992–998. [CrossRef]
6. Gordon, I.E.; Rothman, L.S.; Hill, C.; Kochanov, R.V.; Tan, Y.; Bernath, P.F.; Birk, M.; Boudon, V.; Campargue, A.; Chance, K.V.; et al. The HITRAN2016 molecular spectroscopic database. *J. Quant. Spectrosc. Radiat Transf.* **2017**, *203*, 3–69. [CrossRef]
7. Reagan, J.A.; Cooley, T.W.; Shaw, J.A. Prospects for an Economical, Eye-Safe Water Vapor LIDAR. In Proceedings of the IGARSS'93-IEEE International Geoscience and Remote Sensing Symposium, Tokyo, Japan, 18–21 August 1993; pp. 872–874.
8. Machol, J.L.; Ayers, T.; Schwenz, K.T.; Koenig, K.W.; Hardesty, R.M.; Senff, C.J.; Krainak, M.A.; Abshire, J.B.; Bravo, H.E.; Sandberg, S.P. Preliminary measurements with an automated compact differential absorption lidar for the profiling of water vapor. *Appl. Opt.* **2004**, *43*, 3110–3121. [CrossRef]
9. Späth, F.; Metzendorf, S.; Behrendt, A.; Wizemann, H.-D.; Wagner, G.; Wulfmeyer, V. Online/offline injection seeding system with high frequency-stability and low crosstalk for water vapor DIAL. *Opt. Commun.* **2013**, *309*, 37–43. [CrossRef]
10. Repasky, K.S.; Moen, D.; Spuler, S.; Nehrir, A.R.; Carlsten, J.L. Progress towards an autonomous field deployable diode-laser-based differential absorption lidar (DIAL) for profiling water vapor in the lower troposphere. *Remote Sens.* **2013**, *5*, 6241–6259. [CrossRef]

11. Spuler, S.M.; Repasky, K.S.; Morley, B.M.; Moen, D.; Hayman, M.; Nehrir, A.R. Field-deployable diode-laser-based differential absorption lidar (DIAL) for profiling water vapor. *Atmos. Meas. Tech.* **2015**, *8*, 1073–1087. [CrossRef]
12. Spuler, S.; Repasky, K.; Morley, B.; Moen, D.; Weckwerth, T.; Hayman, M.; Nehrir, A. Advances in Diode-Laser-Based Water Vapor Differential Absorption Lidar. In Proceedings of the 27th International Laser Radar Conference (ILRC 27), the EPJ Web of Conferences. New York, NY, USA, 5–10 July 2015; Volume 119, p. 2003.
13. Spuler, S.; Repasky, K.; Hayman, M.; Nehrir, A. Micro-pulse, differential absorption lidar (dial) network for measuring the spatial and temporal distribution of water vapor in the lower atmosphere. In Proceedings of the 28th International Laser Radar Conference (ILRC 28), the EPJ Web of Conferences. Bucharest, Romania, 25–30 June 2017; Volume 176, p. 05012.
14. Spuler, S.M.; Hayman, M.; Stillwell, R.A.; Carnes, J.; Bernatsky, T.; Repasky, K.S. Micro Pulse DIAL (MPD)—A Diode-Laser-Based Lidar Architecture for Quantitative Atmospheric Profiling. *Atmos. Meas. Tech. Discuss.* **2021**, *14*, 4593–4616. [CrossRef]
15. Weckwerth, T.M.; Weber, K.J.; Turner, D.; Spuler, S.M. Validation of a Water Vapor Micropulse Differential Absorption Lidar (DIAL). *J. Atmos. Ocean. Technol.* **2016**, *33*, 2353–2372. [CrossRef]
16. Vu, T.N.; Klehr, A.; Sumpf, B.; Wenzel, H.; Erbert, G.; Tränkle, G. Wavelength stabilized ns-MOPA diode laser system with 16 W peak power and a spectral line width below 10 pm. Semicond. *Sci. Technol.* **2014**, *29*, 035012. [CrossRef]
17. Vu, T.N.; Klehr, A.; Sumpf, B.; Wenzel, H.; Erbert, G.; Tränkle, G. Tunable 975 nm nanosecond diode-laser-based master-oscillator power-amplifier system with 16.3 W peak power and narrow spectral linewidth below 10 pm. *Opt. Lett.* **2014**, *39*, 5138–5141. [CrossRef]
18. Fricke, J.; Klehr, A.; Brox, O.; John, W.; Ginolas, A.; Ressel, P.; Weixelbaum, L.; Erbert, G. Y-branch coupled DFB-lasers based on high-order Bragg gratings for wavelength stabilization. Semicond. *Sci. Technol.* **2013**, *28*, 035009. [CrossRef]
19. Tawfieq, M.; Fricke, J.; Müller, A.; Della Casa, P.; Ressel, P.; Ginolas, A.; Wenzel, H.; Sumpf, B.; Tränkle, G. Characterization and comparison between different S-bend shaped GaAs Y-branch distributed Bragg reflector lasers emitting at 976 nm. *Semicond. Sci. Technol.* **2018**, *33*, 115001. [CrossRef]
20. Sumpf, B.; Fricke, J.; Ginolas, A.; Maassdorf, A.; Maiwald, M.; Müller, A.; Tawfieq, M.; Theurer, L.S.; Vu, N.T.; Wenzel, H. Tunable Y-branch dual-wavelength diode lasers in the VIS and NIR range for sensor applications. In *Novel In-Plane Semiconductor Lasers XVIII*; SPIE: San Francisco, CA, USA, 2019; Volume 10939, p. 1093913.
21. Chevillard, J.P.; Mandin, J.Y.; Flaud, J.M.; Camy-Peyret, C. Line positions and intensities between 9500 and 11,500 cm^{-1}. The interacting vibrational states (041), (220), (121), (022), (300), (201), (102), and (003). *Can. J.Phys.* **1989**, *67*, 1065–1084. [CrossRef]
22. Fricke, J.; John, W.; Klehr, A.; Ressel, P.; Weixelbaum, L.; Wenzel, H.; Erbert, G. Properties and fabrication of high-order Bragg gratings for wavelength stabilization of diode lasers. *Semicond. Sci. Technol.* **2012**, *27*, 055009. [CrossRef]
23. Fricke, J.; Bugge, F.; Ginolas, A.; John, W.; Klehr, A.; Matalla, M.; Erbert, G. High-power 980-nm broad-area lasers spectrally stabilized by surface Bragg gratings. *IEEE Photonics Technol. Lett.* **2010**, *22*, 284–286. [CrossRef]
24. Brox, O.; Bugge, F.; Ginolas, A.; Klehr, A.; Ressel, P.; Wenzel, H.; Erbert, G.; Trankle, G. High-power ridge waveguide DFB and DFB-MOPA lasers at 1064 nm with a vertical farfield angle of 15°. In *Novel In-Plane Semiconductor Lasers IX*; SPIE OPTO: San Francisco, CA, USA, 2010; Volume 7616, p. 761610.
25. Wenzel, H.; Fricke, J.; Klehr, A.; Knauer, A.; Erbert, G. High-power 980-nm DFB RW lasers with a narrow vertical far field. *IEEE Photon Technol. Lett.* **2006**, *18*, 737–739. [CrossRef]
26. Liero, A.; Klehr, A.; Schwertfeger, S.; Hoffmann, T.; Heinrich, W. Laser driver switching 20 A with 2 ns pulse width using GaN. In Proceeding of the 2010 IEEE MTT-S International Microwave Symposium, Anaheim, CA, USA, 23–28 May 2010; pp. 1110–1113.
27. SpieBberger, S.; Schiemangk, M.; Wicht, A.; Wenzel, H.; Brox, O.; Erbert, G. Narrow Linewidth DFB Lasers Emitting Near a Wavelength of 1064 nm. *J. Light. Technol.* **2010**, *28*, 2611–2616. [CrossRef]
28. Spießberger, S.; Schiemangk, M.; Wicht, A.; Wenzel, H.; Erbert, G.; Tränkle, G. DBR laser diodes emitting near 1064 nm with a narrow intrinsic linewidth of 2 kHz. *Appl. Phys. A* **2011**, *104*, 813–818. [CrossRef]
29. Spießberger, S.; Schiemangk, M.; Sahm, A.; Wicht, A.; Wenzel, H.; Peters, A.; Tränkle, G. Micro-integrated 1 Watt semiconductor laser system with a linewidth of 3.6 kHz. *Opt. Express* **2011**, *19*, 7077–7083. [CrossRef] [PubMed]
30. Sahm, A.M.; Thiem, H.; Paschke, K.; Fricke, J.; Knauer, A.; Erbert, G. 4.5 W hybrid integrated master-oscillator power-amplifier at 976 nm on micro-optical bench. In *Photonics Packaging, Integration, and Interconnects IX*; Integrated Optoelectronic Devices; SPIE OPTO: San Jose, CA, USA, 2009; Volume 7221.